HHS Public Access

Author manuscript

Ultrasound Med Biol. Author manuscript; available in PMC 2017 February 01.

Published in final edited form as:

Ultrasound Med Biol. 2016 February ; 42(2): 607–618. doi:10.1016/j.ultrasmedbio.2015.09.024.

Toward three-dimensional echocardiographic determination of regional myofiber structure

Michelle L. Milne[1], **Gautam K. Singh**[2], **James G. Miller**[2], **Kirk D. Wallace**[3], and **Mark R. Holland**[4]

[1]St. Mary's College of Maryland, St. Mary's City, MD, USA

[2]Washington University in St. Louis, Saint Louis, MO, USA

[3]GE Global Research, Niskayuna, NY, USA

[4]Indiana University School of Medicine, IUPUI, Indianapolis, IN, USA

Abstract

As a step toward the goal of relating changes in underlying myocardial structure to observed altered cardiac function in the hearts of individual patients, this study addresses the feasibility of creating echocardiography-derived maps of regional myocardial fiber structure for entire, intact, excised sheep hearts. Backscatter data were obtained from apical echocardiographic images acquired with a clinical ultrasonic imaging system and used to determine local fiber orientations in each of seven hearts. Systematic acquisition across the entire heart volume provided information sufficient to give a complete map for each heart. Results from the echocardiography-derived fiber maps compare favorably with corresponding results derived from diffusion tensor magnetic resonance imaging. The results of this study provide evidence of the feasibility of using echocardiographic methods to generate individualized whole heart fiber maps for patients.

Keywords

Anisotropy; Heart; Echocardiography; Fiber Structure; Myocardium

Introduction

In the heart, function and structure are closely linked (Arts et al. 2003; Buckberg et al. 2008; Sengupta et al. 2006; Sengupta et al. 2007) and, as a consequence, knowledge of the specific myocardial fiber structure throughout the heart of an individual patient could aid in the identification of the origin of dysfunction, as well as in evaluating the potentially beneficial effects of therapy. To this end, the advancement of methods to image intrinsic myocardial structure has been identified as a key area of development in recommendations from the

Corresponding author: Michelle L. Milne, Physics Department, St. Mary's College of Maryland, St. Mary's City, MD, 20653, USA. mlmilne@smcm.edu.

National Heart, Lung and Blood Institute (NHLBI). (Baumgartner et al. 2005; Buckberg et al. 2004; Williams et al. 2006) Alterations in myocardial fiber structure and orientation can also precede cardiac dysfunction and the clinical manifestation. (Giglio et al. 2003) Mapping the fiber structure of the whole heart would provide insight into both global and regional function and could potentially permit a better understanding of the role that the underlying myocardial structure is playing in the individual's cardiac function and as well as creating the opportunity for early intervention for a better outcome. (Arts et al. 2003; Buckberg et al. 2008; Costa et al. 2001; McQueen and Peskin 2000; Peskin and McQueen 1992; Sengupta et al. 2006; Sengupta et al. 2007) Such information could be useful in identifying subclinical alterations in fiber structure and thus create the opportunity for early intervention for a better outcome. Furthermore, assessment of fiber orientation may provide additional insights into the origin of observed altered global and regional cardiac deformation as currently assessed by advanced methods such as *in vivo* wall motion tracking methods and, hence, provide additional diagnostic information. To this end, efforts have been made to map the fiber structure of the heart using modalities such as diffusion tensor imaging (DTI) and elastic tensor imaging (ETI).(Lee et al. 2012a; Lee et al. 2012b) Therefore, one of the motivations behind this study is to contribute to the development of a method that will permit a better understanding of the role fiber structure plays in the overall cardiac function in individual patients.

Ultrasonic imaging is well suited as a modality for generating myocardial fiber maps for the individual patient. Ultrasound is widely available and utilized in routine clinical practice for decision making and is relatively inexpensive. It does not involve ionizing radiation and thus is well-suited for serial evaluations. Although this approach would be useful in observing the undesirable remodeling associated with myocardial infarction, its primary contribution is likely to in monitoring (constructive) reverse remodeling such as that seen in resynchronization therapy (Mekkaoui et al. 2012; Yu et al. 2002) or potential reverse-remodeling observed in heart failure patients utilizing left ventricular assist devices (LVAD) and therefore monitoring the efficacy of therapy. (Ambardekar and Buttrick 2011; Hellawell and Margulies 2012). In children born with single ventricle physiology, staged palliation employing the single ventricle to support the systemic circulation has resulted in remarkable survival of children with a heart defect otherwise proving uniformly fatal if not repaired with this palliation (Cetta et al. 1996; Gaynor et al. 2002). However, in many, the palliation fails due to single ventricular failure (Khairy et al. 2008) that arises partly from abnormal myocardial fiber architecture and fibrous matrix of the ventricular myocardium (Ho et al. 1996). A study of single ventricle myocardial fiber orientation may help patient and appropriate intervention selection. This is often hampered by a lack of non-invasive and easy to use tool to study the myocardial fiber architecture.

To this end a previous report from our laboratory demonstrated that, in principle, quantitative measurements of myocardial fiber structure for individual hearts can be derived from analyses of echocardiographic images. (Milne et al. 2012) That study, limited to 2D short-axis reconstructions, found that echocardiographic-based measurements of fiber structure in a specific transverse plane qualitatively agreed with the corresponding estimates obtained using diffusion tensor magnetic resonance imaging (MRI) methods. The objective

of the current study is to extend the previous work on single planes of the heart by demonstrating the feasibility of creating quantitative myofiber multiplane structure maps over the entire volume of intact hearts based on 3D echocardiographic information. In addition, our echocardiographic-derived estimates are quantitatively compared with published diffusion MRI measurements of fiber structure. Regional differences in fiber structure within the heart are also elucidated for selected regions-of-interest (ROI).

Methods

Seven sheep hearts were obtained within one hour of slaughter from a local slaughterhouse using a procedure consistent with the policies of the Animal Studies Committee of Washington University. Sheep hearts were utilized because they are comparable in size and composition to the human heart. (Rudolph 2009) The intact, excised hearts were thoroughly rinsed and fixed in a 10% formalin solution for a minimum of five weeks prior to being imaged. The use of fixed tissue permitted ample time for imaging of the hearts without concerns for structural degradation. (Some limitations arising from the use of fixed tissue are described below in the Discussion section.)

Methods for data acquisition and analysis were similar to the methods described in a previous paper from our laboratory. (Milne et al. 2012) In brief, after fixation preparation was completed, each heart was placed base-down in a cylindrical water-filled tank in preparation for collecting backscatter data. A series of apical echocardiographic images, in 5-degree rotational increments about the apex of each heart, were obtained using a General Electric Vivid 7 clinical imaging system (GE Healthcare, Wauwatosa, WI, USA) at a nominal center frequency of 5.0 MHz in fundamental imaging mode (Figure 1a). A GE Model 7S phased-array probe was used in fundamental imaging mode at 5.0 MHz nominal frequency. The postprocessing settings on the clinical imaging system were configured such that the grayscale level of the images had a linear relationship to the amount of backscattered energy, to allow quantitative estimates of the level of backscatter from the grayscale images. The details of this calibration have been previously described by our laboratory. (Holland et al. 2006) The time-gain compensation (TGC) settings were adjusted so that the backscatter signal strength was within the useful linear dynamic range for all depths and a single transmit focus was placed near the center of the left ventricle.

After image acquisition, the backscatter values along individual transverse profile lines corresponding to specific depths from the apex were normalized using the following approach: Myofibers that are perpendicular to the ultrasound beam (typically fibers in the mid-myocardium) are known to yield the largest acoustic backscatter values. (Hoffmeister et al. 1995; Holland et al. 1997; Yang et al. 2007) Consequently, at a specific distance from the apex, the pixels with the highest values of backscatter along transverse profile lines placed on the left and right walls of the heart in the grayscale image were identified as arising from locations where the fiber orientation was predominately perpendicular to the ultrasonic beam direction. These brightest pixels were normalized to the maximum gray scale value and all other pixels were normalized to their corresponding relative gray scale value. Normalizing the backscatter in this fashion provided an approach to compensate for the effects of signal attenuation as the acoustic beam traveled through the overlying tissue in a fashion that is

analogous to transthoracic apical window imaging in a clinical setting (Figure 1b). Possible issues arising from the assumption that the brightest pixels correspond to fiber orientations perpendicular to the ultrasonic beam are considered in the Discussion section below.

After normalization, fiber angle relative to the beam direction was determined from the normalized backscatter values. This determination was carried out by making use of previously acquired backscatter data relating the magnitude of the scattered signal to the orientation of the acoustic beam relative to the fiber direction. (Milne et al. 2012) In this previous study, cylindrical myocardial cores from an additional set of fixed sheep hearts were insonified from different angles using the same clinical echocardiographic imaging system configured in the same fashion as described above. The resulting grayscale images and the relative core/ultrasonic probe orientation data were analyzed to relate signal strength to fiber direction relative to the interrogating acoustic beam (Figure 1c).

In the current study, with the information obtained from all distances from the apex of the heart, the fiber angle data were combined into a single, three-dimensional, composite fiber map for each heart. Fiber orientation was interpolated to fill in the regions between each acquired apical echocardiographic view in order to create a complete three-dimensional fiber angle map of the heart. This interpolation was accomplished by bisecting the gap between the apical views and filling with a weighted average of the nearest neighbors, in a fashion similar to that used to fill the gaps in the “fan” of a clinical echocardiogram sector image. The distributions of fiber orientations were determined for specific regions-of-interest, thus permitting comparison among different regions of the heart and to permit comparison of our data with previously published findings.

Results

For each of the seven hearts that were studied, the fiber orientation relative to the direction of the ultrasound beam, which roughly parallels the long axis of the heart, was obtained for the entire heart as described above. Figure 2 illustrates how data were reassembled for one of the hearts in the manner depicted in the accompanying cartoon and for comparison includes the equivalent fiber map obtained by diffusion MRI for the same levels of the same heart. Figure 3 shows the percent difference in measured fiber orientation between the two imaging modalities. In general the percent difference between the fiber angles measured using the two modalities is less than 15% in the mid-myocardium tissue of the left ventricular wall. This reported difference is likely an upper limit on the true disagreement between the two methods, because the disagreement is largely associated with the difficulty of achieving proper registration between the images. Figure 4 shows the same transverse slices depicted in Figure 2 (plus one additional transverse slice from the base of the heart) side-by-side for easier inspection of the fiber orientation. Figure 5 shows the data from the same heart reassembled in a three-plane view. The same three-plane view for the remaining six hearts used in this study are displayed in Figure 6.

For each heart, these data indicate that the fibers in the midmyocardium are typically oriented circumferentially (corresponding to a helical angle of 0° and a gray scale value of maximally white in the images). The fibers exhibited gradually increasing tilt angles as the

location moves towards the endocardium or towards the epicardium (corresponding to increasing helical fiber angles and darker gray scale values). This orientation appears to be consistent with reported results obtained by histological assessment of myocardial fiber orientation (Greenbaum et al. 1981; Streeter et al. 1969). For one heart, a second set of ultrasound data was taken at a later date and the fiber orientation analysis was repeated. Examining a selection of regions in the two fiber maps acquired on the two separate occasions showed that variation between the fiber angles for the same tissue was less than 10 degrees on average. As with the comparison between the ultrasonic fiber maps and diffusion MRI fiber maps, comparison was complicated by the difficulty of properly co-registering the images, hence the true variability in the fiber maps may be considerably less. It should also be noted that with histological assessment, the standard deviation for myofiber at a given location is found to be approximately 5 degrees on average (Greenbaum et al. 1981; Streeter et al. 1969)

Transmural profile lines, such as those shown in Figure 7, demonstrate in greater detail the change in orientation of fiber angle across the myocardial walls. These profile lines were generated from two regions in the heart, one more apical and one more basal, and in two views, one similar to the four chamber view and one similar to the two chamber view. All four profile lines demonstrate the gradual rotation of fiber angle for transmural locations within the heart wall. For example, for a progression beginning at an orientation of approximately 60° at the epicardium of the left ventricular free wall, the profile lines show the fibers gradually rotating toward an orientation of 0° (i.e. circumferential) in the mid-myocardial region, and then gradually rotating away from circumferential back toward an angle of approximately 60° as one travels toward the endocardium of the left ventricular freewall.

Discussion

In Figure 8, results of the present study are compared with those from a previously published study of sheep hearts (Mekkaoui et al. 2012) obtained using diffusion tensor MRI. These data correspond to an area of interest in the midlevel of the left ventricular free wall. In order to facilitate direct comparison, results from our study are plotted in a manner such that fibers exhibit a right-handed helical orientation closer to the endocardium (i.e. the angle is positive in the subendocardial region) and a left-handed helical orientation closer to the epicardium (i.e. negative in the subepicardial region), which is to say that the appropriate sign was assigned to the calculated magnitude of the fiber orientation for purposes of comparison. For normal hearts and hearts with only mild fiber orientation disorder, we expect that sign assignment should be straightforward; however, it may become more problematic in severely diseased hearts. In the Mekkaoui paper, the reconstructed myofiber lengths were limited to half the heart circumference (defined as the πR case in the Mekkaoui paper). Median values from the Mekkaoui paper are shown with a dashed line in Figure 8, with minimum and maximum angles shown with dotted lines. The fiber angles are plotted as functions of position measured as a percentage of the distance through the left ventricular free wall for both studies. Data from the current study are shown using a solid line; error bars denote the standard deviation at each position. Data from the current echocardiography-based study are in good agreement with those obtained with diffusion tensor MRI.

Furthermore, the transmural distribution of fiber angles observed in the current study are similar to the histology-derived values observed in canine hearts (Streeter et al. 1969) and in human hearts (Greenbaum et al. 1981).

When comparing an ultrasonic method of obtaining fiber orientation to fiber orientation obtained with diffusion tensor MRI, it is useful to note the strengths and weaknesses of each modality. One primary limitation of diffusion MRI is the relatively long scan time required to obtain a high-resolution image. For this reason, the MRI fiber map shown in figure 2 has a much lower spatial resolution that its ultrasonic counterpart. In addition, MRI also suffers from susceptibility artifacts, which appear primarily at the edge of the tissue. In this study, efforts were made to minimize potential susceptibility artifacts using a spin-echo sequence. We expect susceptibility artifacts would be less prominent in *in vivo* studies because the heart tissue is not surrounded by air. Ultrasound is faster and has higher resolution, however one drawback is the inherent inability to distinguish between fibers that are rotated *towards* the ultrasonic beam from fibers that are rotated the same angle *away* from the ultrasonic beam with respect to the perpendicular plane. Such a distinction may require additional images to be acquired using different echocardiographic windows.

In Figure 9 the distribution of fiber angles associated with specific regions of the heart (left ventricular free wall, right ventricular free wall, and septum) are presented. The differences in the fiber orientation distributions observed in the right, septal, and left ventricular regions are likely associated with the different roles each myocardial region plays in overall cardiac function. These data demonstrate that the tissues in the left ventricular free wall tend to have more fibers at low angles (below 20°) and a distribution which peaks between 21° and 30° (*i.e.*, consistent with more circumferentially oriented fibers and a radial contraction). In contrast, fibers in the right ventricular free wall exhibit distributions with peaks between 31° and 40° (i.e., more longitudinally oriented fibers). The fiber angle distribution for the septal wall lies between those of the two outer walls, perhaps a consequence of the sharing of the septal wall between the right and left ventricles and thus sharing characteristics, as well as functions, of both the right and left ventricular walls.

To assess the potential clinical implementation of echocardiography-based estimates of fiber orientation, we explored the use of real-time 3D volumetric echocardiographic imaging. A GE Vivid E9 imaging system, equipped with a 4V matrix phased array transducer, was used to acquire complete volumetric images of one of the sheep hearts from a single position and orientation of the probe. In an analogous configuration to the one described above, the heart was placed base-down in a water bath and interrogated from the apex, as depicted in Figure 10. Figure 11 depicts a transverse cut-away rendered view of the 3D volume of backscatter data, where the bright midmyocardial region is clearly delineated. Figure 12 shows a series of nine individual transverse image planes extracted from the 3D volumetric acquisition, tiled in a fashion similar to that shown in Figure 4. Although these data do not explicitly represent the measured fiber orientations, similarities between Figure 12 and Figure 4 (*i.e.*, the bright band in the midmyocardium and gradual change in brightness as one moves towards the epicardial and endocardial regions) are striking. These results, therefore, suggest eventual clinical implementation of echocardiography-based estimates of fiber orientation (in beating hearts) using 3D volumetric imaging methods may be feasible. In Figure 13, line

profiles at one level of the 3D ultrasonic date are presented. These images are qualitatively similar to the basal line profiles for the 2D ultrasonic data presented in Figure 6 (the 3D system was not specifically configured to have a linear relationship between grayscale brightness and backscatter level, hence the relationship between backscatter level and fiber orientation could not be quantified). Fully translating this approach to 3D echocardiography may require trade-offs between optimal volume acquisition rates and spatial resolution. If higher spatial resolution is needed, image acquisition could be ECG triggered and the fiber map generated from a composite volume acquired over multiple heart cycles.

There are some limitations associated with the echocardiographic approach employed in this study. An inherent limitation of ultrasonic imaging is the spatial variations in signal intensity (speckle) (Wagner et al. 1983), which contributed to apparent spatial variations in the estimated fiber orientation. Spatial averaging serves to reduce the potential consequences of speckle on estimates of fiber orientation. (Baldwin et al. 2005; Liu and Zagzebski 2010) Although this spatial averaging reduces the effective resolution of our method, results seen in Figures 2 through 8 clearly indicate the gradation of fiber orientation, as expected. In addition, a single transmit focus was utilized for these studies. Utilization of multiple focal zones may potentially enhance the spatial resolution of fiber orientation estimation but may adversely affect the required frame rates necessary for *in vivo* measurements.

We have chosen to use fixed tissue in this preliminary study to avoid the additional complication of changes in tissue properties during the imaging process. Although fixation is known to affect some ultrasonic properties of the tissue, such as the attenuation (Hall et al. 2000), it is generally assumed that fixation does not significantly alter fiber orientation, which is of primary interest for this study.

In addition, the fiber angle was measured relative to the direction of the ultrasonic beam, which roughly parallels the walls of the heart. A more sophisticated approach may be to report the fiber orientation based on a heart-defined coordinate system. This approach was not attempted in this preliminary study. However, a trigonometric calculation suggests that the maximum error is less than 10 degrees in the apical region for all the hearts studied, and is less than 5 degrees in the middle and base of the hearts using the current (beam-based geometry) method.

We anticipate that the methods used here could also be used in *in vivo* hearts without substantial change, so long as the data were processed frame by frame. A potential complication in the clinical application might appear for hearts where fiber orientation has been substantially altered, as this might invalidate the assumption that the brightest backscatter in a given level of the heart corresponded to fibers normal to the ultrasonic beam. Nonetheless, this alteration should be readily identifiable when compared to that anticipated for normal fiber structure and may provide useful diagnostic information.

Conclusion

Results of this study demonstrate the feasibility of imaging the myofiber structure of whole hearts using echocardiographic methods. The fiber maps created during this study are

consistent with previously reported histological results as well as with the fiber orientation obtained by diffusion magnetic resonance (Mekkaoui et al. 2012; Milne et al. 2012), suggesting that the fiber orientation estimated from echocardiography can provide a quantitative assessment of the unique fiber orientations associated with specific regions of the heart.

Acknowledgments

Helpful comments and suggestions by Professor Jonathan I. Katz are sincerely appreciated. This work was supported in part by NIH grants R01 HL40302 and R21 HL106417.

References

Ambardekar A, Buttrick P. Reverse remodeling with left ventricular assist devices: a review of clinical, cellular, and molecular effects. Circ Heart Fail. 2011; 4:224–33. [PubMed: 21406678]

Arts T, Bovendeerd P, Delhaas T, Prinzen F. Modeling the relation between cardiac pump function and myofiber mechanics. J Biomech. 2003; 36:731–6. [PubMed: 12695003]

Baldwin SL, Holland MR, Sosnovik DE, Miller JG. Effects of Region-of-Interest Length on Estimates of Myocardial Ultrasonic Attenuation and Backscatter. Med Phys. 2005; 32:418–426. [PubMed: 15789588]

Baumgartner WA, Burrows S, del Nido PJ, Gardner TJ, Goldberg S, Gorman RC, Letsou GV, Mascette A, Michler RE, Puskas JD, Rose EA, Rosengart TK, Sellke FW, Shumway SJ, Wilke N. Recommendations of the National Heart, Lung, and Blood Institute Working Group on Future Direction in Cardiac Surgery. Circulation. 2005; 111:3007–13. [PubMed: 15939834]

Buckberg GD, Weisfeldt ML, Ballester M, Beyar R, Burkhoff D, Coghlan HC, Doyle M, Epstein ND, Gharib M, Ideker RE, Ingels NB, LeWinter MM, McCulloch AD, Pohost GM, Reinlib LJ, Sahn DJ, Sopko G, Spinale FG, Spotnitz HM, Torrent-Guasp F, Shapiro EP. Left ventricular form and function: scientific priorities and strategic planning for development of new views of disease. Circulation. 2004; 110:e333–6. [PubMed: 15466651]

Buckberg G, Hoffman JI, Mahajan A, Saleh S, Coghlan C. Cardiac mechanics revisited: the relationship of cardiac architecture to ventricular function. Circulation. 2008; 118:2571–87. [PubMed: 19064692]

Cetta F, Feldt RH, O'Leary PW, Mair DD, Warnes CA, Driscoll DJ, Hagler DJ, Porter C-BJ, Offord KP, Schaff HV, Puga FJ, Danielson GK. Improved early morbidity and mortality after Fontan operation: The mayo clinic experience, 1987 to 1992. J Am Coll Cardiol. 1996; 28:480–486. [PubMed: 8800129]

Costa KD, Holmes JW, McCulloch AD. Modelling cardiac mechanical properties in three dimensions. Phil Trans R Soc Lond A. 2001; 359:1233–1250.

Gaynor JW, Bridges ND, Cohen MI, Mahle WT, DeCampli WM, Steven JM, Nicolson SC, Spray TL. Predictors of outcome after the Fontan operation: Is hypoplastic left heart syndrome still a risk factor? J Thorac Cardiovasc Surg. 2002; 123:237–245. [PubMed: 11828282]

Giglio V, Pasceri V, Messano L, Mangiola F, Pasquini L, Dello Russo A, Damiani A, Mirabella M, Galluzzi G, Tonali P, Ricci E. Ultrasound tissue characterization detects preclinical myocardial structural changes in children affected by Duchenne muscular dystrophy. J Am Coll Cardiol. 2003; 42:309–316. [PubMed: 12875769]

Greenbaum RA, Ho SY, Gibson DG, Becker AE, Anderson RH. Left Ventricular Fibre Architecture in Man. Br Heart Journ. 1981; 45:248–263.

Hall CS, Dent CL, Scott MJ, Wickline SA. High-Frequency Ultrasound Detection of the Temporal Evolution of Protein Cross Linking in Myocardial Tissue. IEEE Trans Ultrason Ferroelec Freq Contr. 2000; 47:1051–1058.

Hellawell JL, Margulies KB. Myocardial Reverse Remodeling. Cardiovasc Ther. 2012; 30:172–181. [PubMed: 21108773]

Hoffmeister BK, Wong AK, Verdonk ED, Wickline SA, Miller JG. Comparison of the Anisotropy of Apparent Integrated Ultrasonic Backscatter from Fixed Human Tendon and Fixed Human Myocardium. J Acoust Soc Am. 1995; 97:1307–1313. [PubMed: 7876450]

Holland MR, Gibson AA, Peterson LR, Areces M, Schaffer JE, Perez JE, Miller JG. Measurements of the Cyclic Variation of Myocardial Backscatter From Two-Dimensional Echocardiographic Images as an Approach for Characterizing Diabetic Cardiomyopathy. J CardioMetabolic Syndr. 2006; 1:149–152.

Holland MR, Hall CS, Lewis SH, Handley SM, Finch-Johnston AE, D'Sa AP, Perez JE, Miller JG. Comparison of Integrated Backscatter Values Obtained Using Acoustic Densitometry with Values Derived from Spectral Analysis of Digitized Signals from a Clinical Imaging System. J Am Soc Echocardiogr. 1997; 10:511–517. [PubMed: 9203490]

Ho SY, Jackson M, Kilpatrick L, Smith A, Gerlis LM. Fibrous Matrix of Ventricular Myocardium in Tricuspid Atresia Compared With Normal Heart A Quantitative Analysis. Circulation. 1996; 94:1642–1646. [PubMed: 8840856]

Khairy P, Fernandes SM, Mayer JE, Triedman JK, Walsh EP, Lock JE, Landzberg MJ. Long-term survival, modes of death, and predictors of mortality in patients with Fontan surgery. Circulation. 2008; 117:85–92. [PubMed: 18071068]

Lee W-N, Larrat B, Pernot M, Tanter M. Ultrasound elastic tensor imaging: comparison with MR diffusion tensor imaging in the myocardium. Phys Med Biol. 2012a; 57:5075–5095. [PubMed: 22836727]

Lee W-N, Pernot M, Couade M, Messas E, Bruneval P, Bel A, Hagège AA, Fink M, Tanter M. Mapping myocardial fiber orientation using echocardiography-based shear wave imaging. IEEE Trans Med Imaging. 2012b; 31:554–562. [PubMed: 22020673]

Liu W, Zagzebski JA. Trade-offs in data acquisition and processing parameters for backscatter and scatterer size estimations. IEEE Trans Ultrason Ferroelectr Freq Control. 2010; 57:340–352. [PubMed: 20178900]

McQueen DM, Peskin CS. A Three-Dimensional Computer Model of the Human Heart for Studying Cardiac Fluid Dynamics. Comput Graph. 2000; 34:56–60.

Mekkaoui C, Huang S, Chen HH, Dai G, Reese TG, Kostis WJ, Thiagalingam A, Maurovich-Horvat P, Ruskin JN, Hoffmann U, Jackowski MP, Sosnovik DE. Fiber architecture in remodeled myocardium revealed with a quantitative diffusion CMR tractography framework and histological validation. J Cardiovasc Magn Reson. 2012; 14:70. [PubMed: 23061749]

Milne ML, Singh GK, Miller JG, Holland MR. Echocardiographic-based assessment of myocardial fiber structure in individual, excised hearts. Ultrason Imaging. 2012; 34:129–141. [PubMed: 22972911]

Peskin CS, McQueen DM. Cardiac fluid dynamics. Crit Rev Biomed Eng. 1992; 20:451–9. [PubMed: 1486785]

Rudolph, A. Congenital Diseases of the Heart: Clinical-Physiological Considerations. 3. Wiley-Blackwell; 2009.

Sengupta PP, Korinek J, Belohlavek M, Narula J, Vannan MA, Jahangir A, Khandheria BK. Left ventricular structure and function: basic science for cardiac imaging. J Am Coll Cardiol. 2006; 48:1988–2001. [PubMed: 17112989]

Sengupta PP, Krishnamoorthy VK, Korinek J, Narula J, Vannan MA, Lester SJ, Tajik JA, Seward JB, Khandheria BK, Belohlavek M. Left ventricular form and function revisited: applied translational science to cardiovascular ultrasound imaging. J Am Soc Echocardiogr. 2007; 20:539–51. [PubMed: 17485001]

Streeter DD, Spotnitz HM, Patel DP, Ross J, Sonnenblick EH. Fiber Orientation in the Canine Left Ventricle during Diastole and Systole. Circ Res. 1969; XXIV:339–347. [PubMed: 5766515]

Wagner RF, Smith SW, Sandrik JM, Lopez H. Statistics of Speckle in Ultrasound B-Scans. Sonics Ultrason IEEE Trans On. 1983; 30:156–163.

Williams RG, Pearson GD, Barst RJ, Child JS, del Nido P, Gersony WM, Kuehl KS, Landzberg MJ, Myerson M, Neish SR, Sahn DJ, Verstappen A, Warnes CA, Webb CL. Report of the National Heart, Lung, and Blood Institute Working Group on research in adult congenital heart disease. J Am Coll Cardiol. 2006; 47:701–7. [PubMed: 16487831]

Yang M, Krueger TM, Holland MR, Miller JG. Anisotropy of the Backscatter Coefficient of Formalin-Fixed Ovine Myocardium. J Acoust Soc Am. 2007; 122:581–586. [PubMed: 17614514]

Yu C-M, Chau E, Sanderson JE, Fan K, Tang M-O, Fung W-H, Lin H, Kong S-L, Lam Y-M, Hill MRS, Lau C-P. Tissue Doppler Echocardiographic Evidence of Reverse Remodeling and Improved Synchronicity by Simultaneously Delaying Regional Contraction After Biventricular Pacing Therapy in Heart Failure. Circulation. 2002; 105:438–445. [PubMed: 11815425]

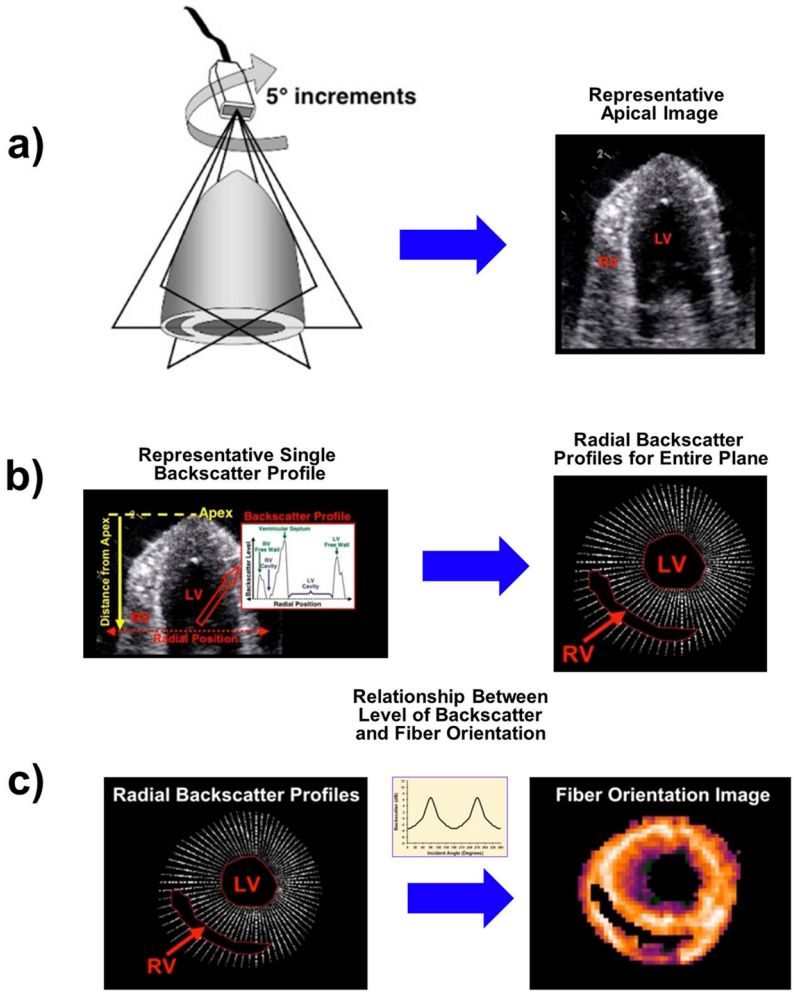

Figure 1.

Generation of fiber orientation estimates within a single short-axis plane: a) A series of apical echocardiographic images were acquired from each excised heart as the probe was systematically rotated in 5° increments over a full 180°. A representative apical image is depicted. b) For each apical image frame acquired, the level of ultrasonic backscatter was measured at each position along a radial line segment positioned a specific distance from the apex. The radial line backscatter profiles corresponding to a specific distance from the apex for each apical echocardiographic image acquired were assembled in the short-axis plane and displayed in a 2D grayscale format. c) The radial line backscatter profile data were transformed into fiber orientation data using a previously measured relationship between the relative level of ultrasonic backscatter and fiber orientation. These data were interpolated and spatially filtered to provide a reconstructed short-axis 2D image depicting local fiber orientation

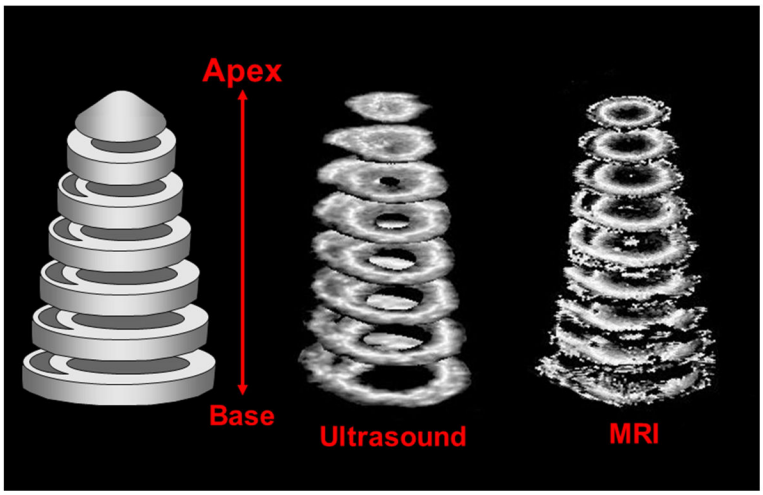

Figure 2.

A cartoon illustration and the corresponding fiber maps for one of the hearts at a selection of levels. The fiber map derived from ultrasonic data is on the left, and the fiber map derived from diffusion MRI data is on the right (note that the two fiber maps have different resolutions). The apex of the heart is at the top of the image; the base of the heart is at the bottom. The large cavity in the center of the basal slices is the left ventricular cavity.

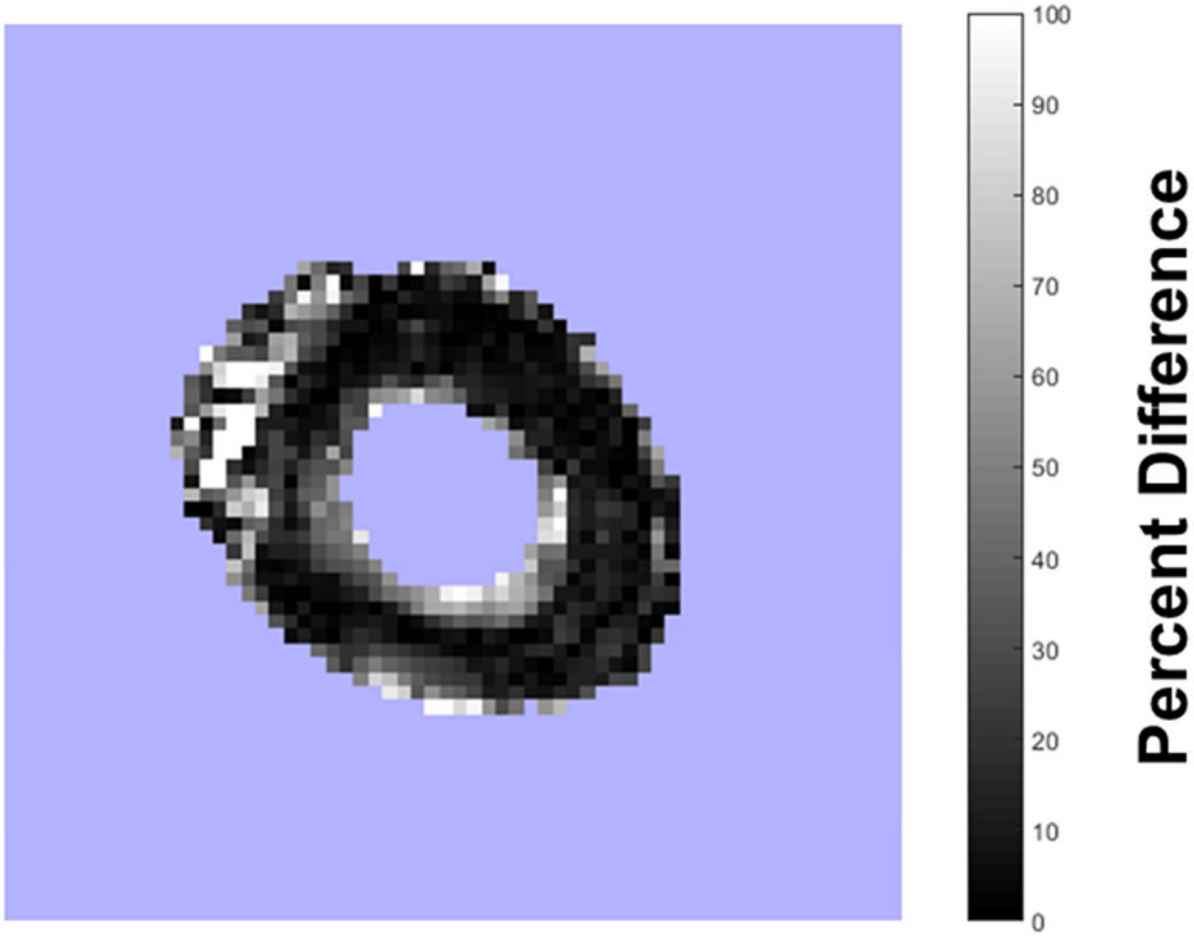

Figure 3.
The percent difference between the fibers for a single layer of one heart as found from ultrasound and diffusion MRI. Note that agreement between the two modalities is particularly good in the mid-myocardium.

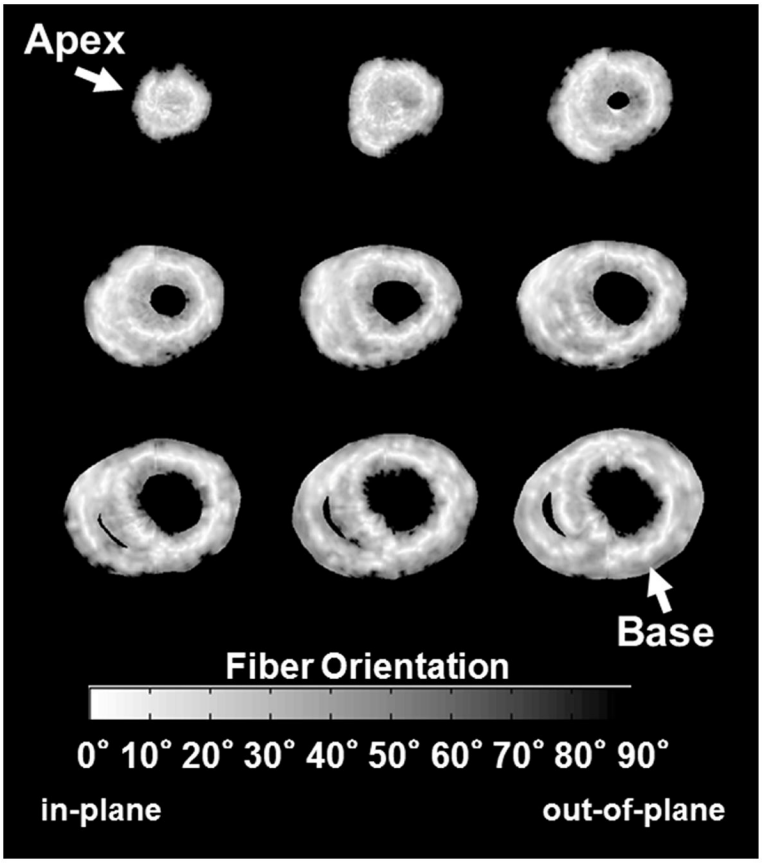

Figure 4.

A series of fiber orientation images corresponding to transverse planes at specific levels of the heart from the apex (top left of figure) to base (bottom right). The central cavity in many of the levels is the left ventricular cavity. Bright white bands in the mid-myocardium result from fibers that have a circumferential orientation (i.e. a fiber orientation of 0°).

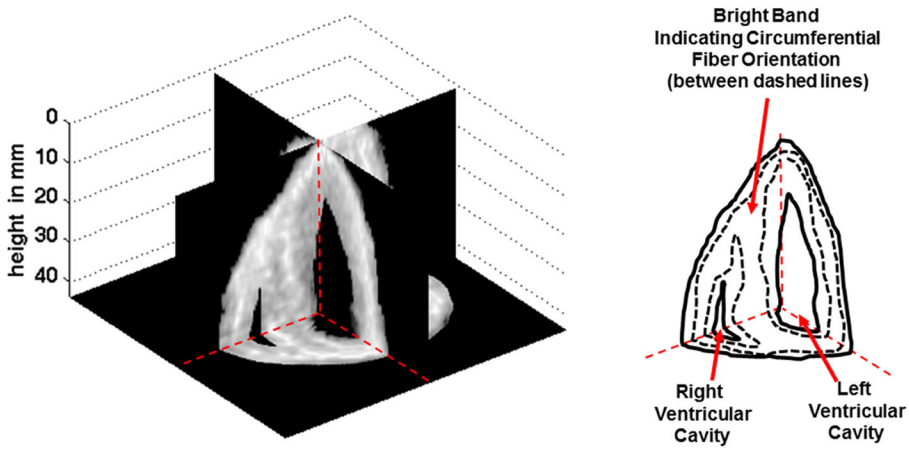

Figure 5.

A three-plane view of the fiber orientation of an excised heart, oriented so that the apex of the heart is at the top of the image. The map on the right shows an outline of the heart tissue (solid lines) and the location of the fibers oriented approximately circumferentially (between the dashed lines).

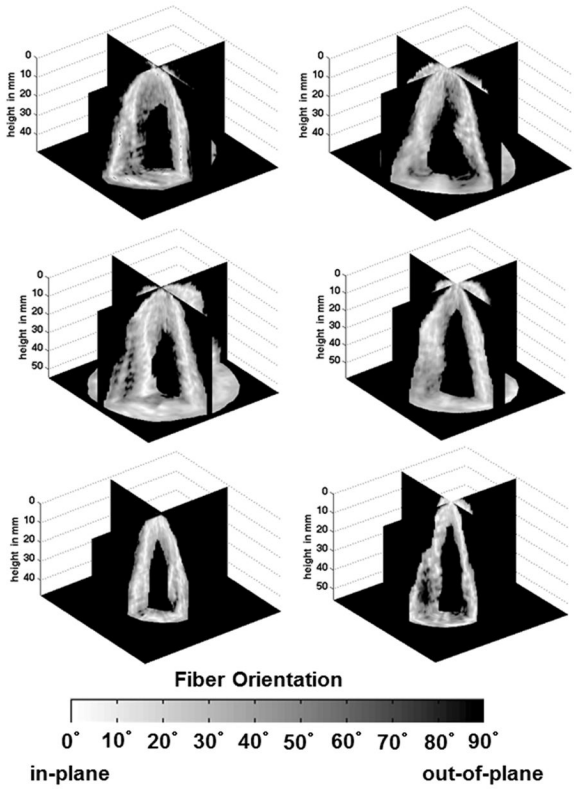

Figure 6.

Three-plane view for the remaining six hearts. Each heart is oriented so that the right ventricle is in the front left of the image. In some cases, the right ventricular cavity is not visible in the image because the cavity lies below the height at which data were taken.

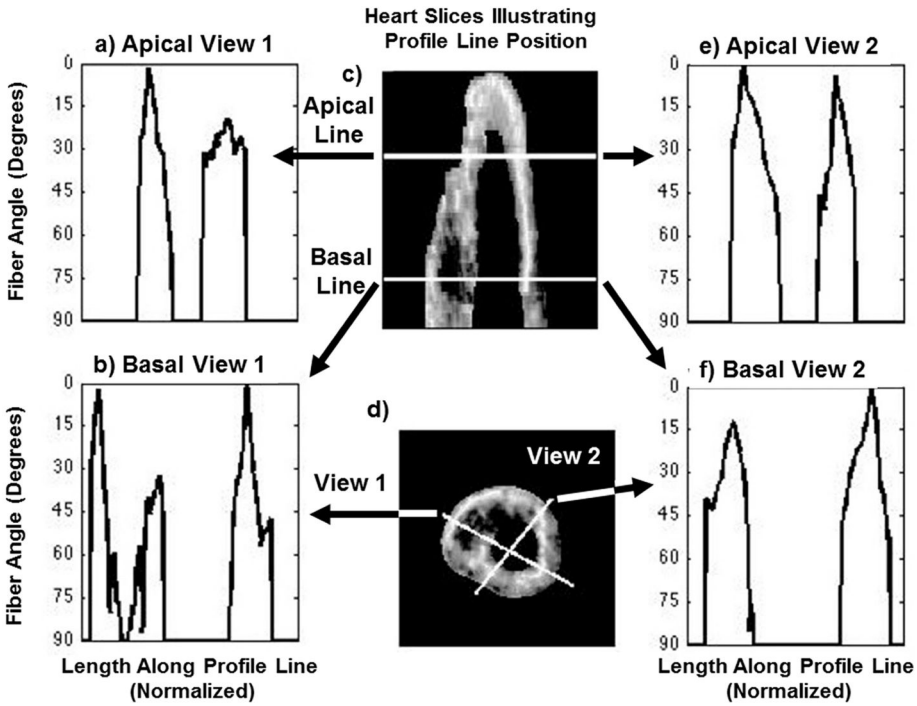

Figure 7.

Transmural profile lines illustrating the fiber orientation at the two levels of the heart shown. At each level, two profiles are presented, as illustrated. In all cases the fiber orientation rotates from an angle greater than 60° towards the 0° (most circumferential) orientation and then back towards higher angles as one travels through each tissue wall. The deep dip in angle shown in the left portion of Basal View 1 corresponds to the location of the right ventricular cavity.

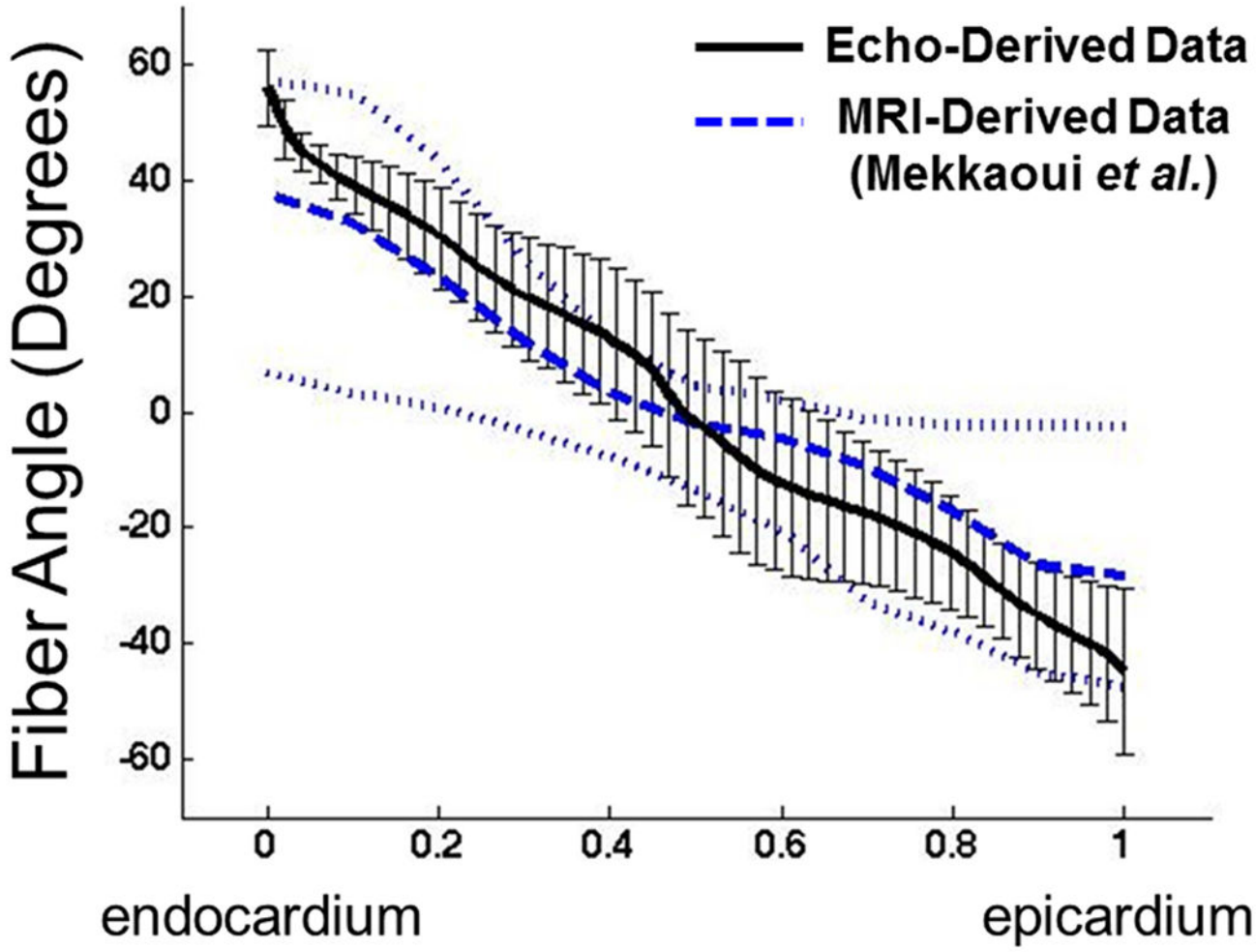

Figure 8.

The results from the current paper are compared with the results from the diffusion tensor MRI-derived study of Mekkaoui (Mekkaoui et al. 2012) Angles are plotted as a function of percent distance through the left ventricular free wall for both sets of data. Current echocardiography-based results are shown with a solid line, with the error bar depicting the standard deviation. The corresponding mean values of the helical angles for the Mekkaoui *et al*. results are shown with a dashed line, with the maximum and minimum angles measured along a fiber shown with dotted lines.

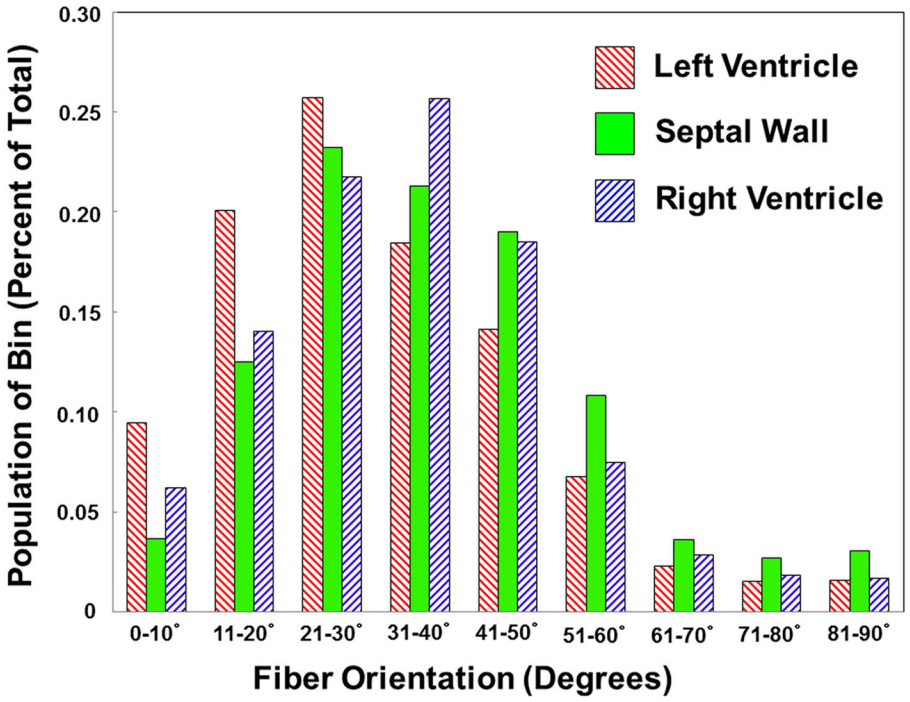

Figure 9.

Comparison of fiber orientations in different regions of the heart. The left ventricular free wall orientations are shown in red (downward hatching lines), the septal wall orientations are shown in green (solid), and the right ventricular free wall orientations are shown in blue (upward hatching lines). The fibers in the left ventricular wall have a slightly shallower average fiber orientation than those in the right ventricular wall.

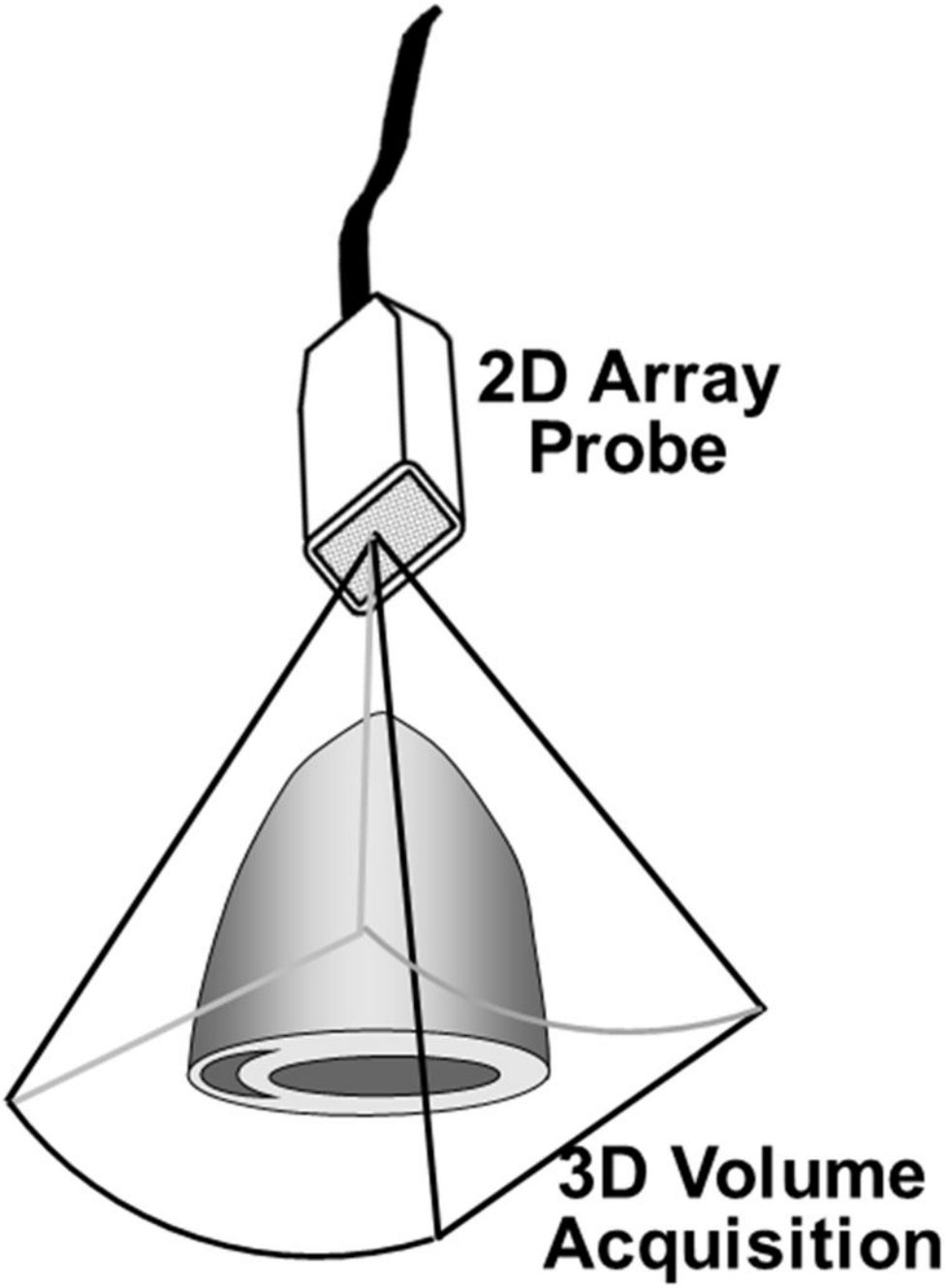

Figure 10.
Cartoon depicting the manner of the 3D volume acquisition of the hearts.

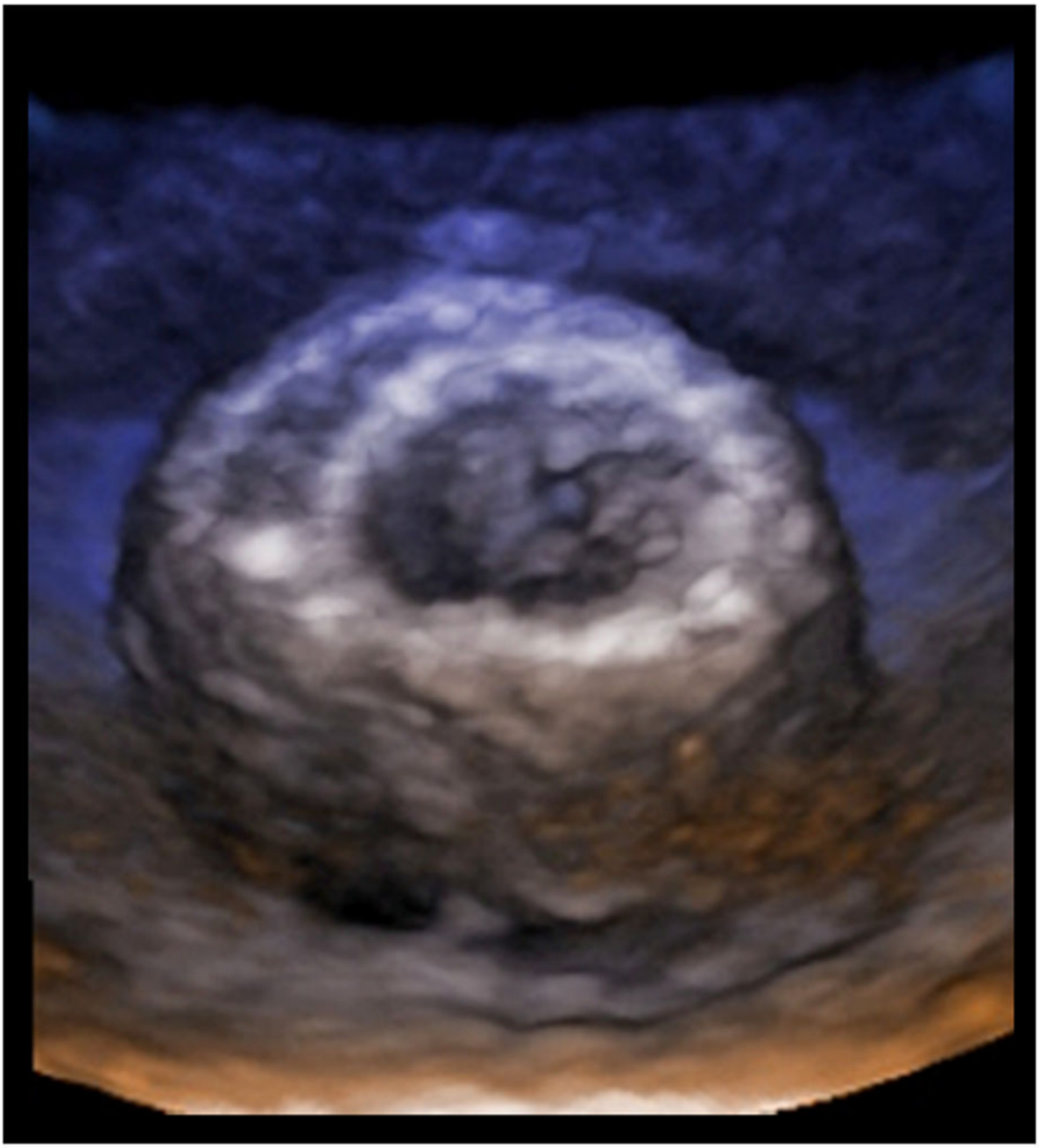

Figure 11.
Volume rendered cut-away image of an excised sheep heart acquired using the 3D echocardiographic imaging system. The bright midmyocardial region, consistent with circumferential fiber orientation, is clearly delineated.

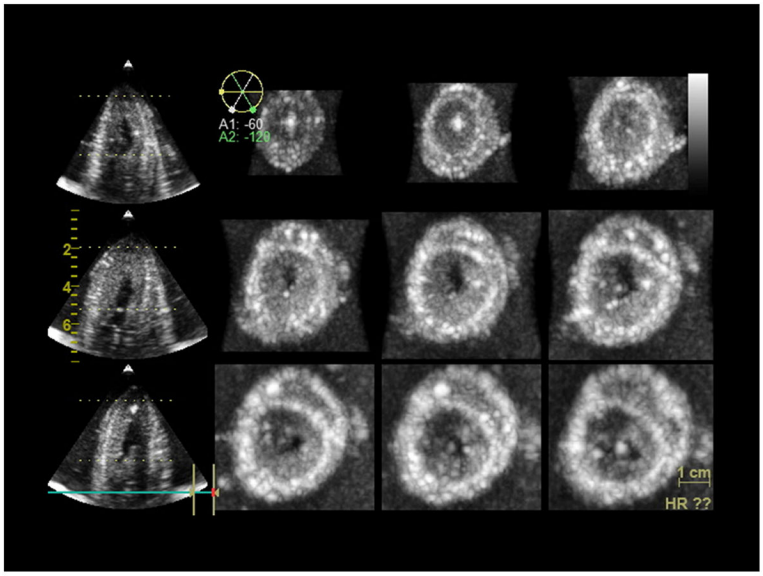

Figure 12.

Series of transverse short-axis slices, from apex to base, extracted from the 3D volumetric echocardiographic data acquired from an excised sheep heart. As in Figure 2, brighter pixels within the mid-myocardium correspond with regions having in-plane fiber orientation.

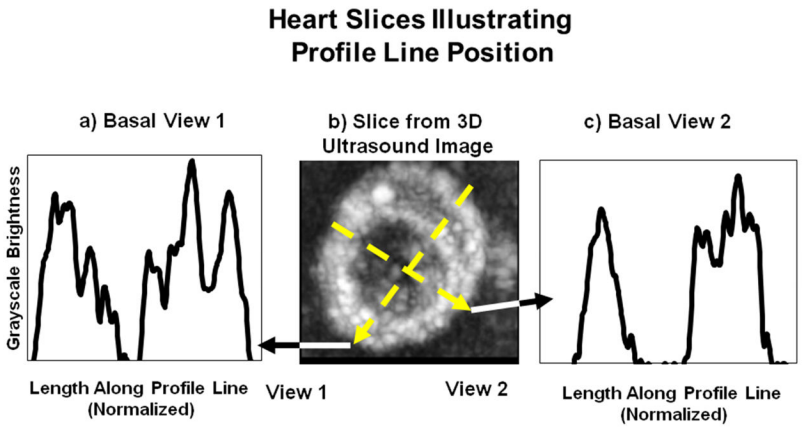

Figure 13.

Line profiles for two views as seen in the 3D ultrasonic data. Note the similarity to the basal views in figure 7.